AGU ADVANCING EARTH AND SPACE SCIENCE

Earth and Space Science

RESEARCH ARTICLE
10.1029/2020EA001463

Moho Depth of Northern Baja California, Mexico, From Teleseismic Receiver Functions

E. E. Ramírez[1], Klaus Bataille[2], J. A. Vidal-Villegas[3], J. M. Stock[4], and J. Ramírez-Hernández[1]

[1]Instituto de Ingeniería, Universidad Autónoma de Baja California (UABC), Mexicali, BC, México, [2]Departamento de Ciencias de la Tierra, Universidad de Concepción, Concepción, Chile, [3]Departamento de Sismología, División Ciencias de la Tierra, Centro de Investigación Científica y de Educación Superior de Ensenada, Ensenada, Baja California, México, [4]Seismological Laboratory, Division of Geological and Planetary Sciences, California Institute of Technology (Caltech), Pasadena, CA, USA

Key Points:

- Moho variations in Northern Baja California
- Receiver functions of stations belonging to the Northwest Mexico seismic network
- Crustal thickness of the Peninsular Ranges of Baja California and the Mexicali Valley

Supporting Information:

Supporting Information may be found in the online version of this article.

Correspondence to:

E. E. Ramírez,
ramirez.erik@uabc.edu.mx

Citation:

Ramírez, E. E., Bataille, K., Vidal-Villegas, J. A., Stock, J. M., & Ramírez-Hernández, J. (2021). Moho depth of northern Baja California, Mexico, from teleseismic receiver functions. *Earth and Space Science*, *8*, e2020EA001463. https://doi.org/10.1029/2020EA001463

Received 14 SEP 2020
Accepted 13 MAR 2021

Abstract We estimated Moho depths from data recorded by permanent and temporary broadband seismic stations deployed in northern Baja California, Mexico, using the receiver function technique. This region is composed of two subregions of contrasting geological and topographical characteristics: the Peninsular Ranges of Baja California (PRBC), a batholith with high elevations (up to 2,600 m); and the Mexicali Valley (MV) region, a sedimentary environment close to sea level. Crustal thickness derived from the *P*-to-*S* converted phases at 29 seismic stations were analyzed in three profiles: Two that cross the two subregions, in ~W-E direction, and the third one that runs over the PRBC in a N-S direction. For the PRBC, Moho depths vary from 35 to 45 km, from 33°N to 32°N; and from 30 to 46 km depth from 32°N to 30.5°N. From a profile that crosses the subregions in the W-E direction; Moho depths vary from 45 to ~34 km under western and eastern PRBC, respectively; with an abrupt change of depth under the Main Gulf Escarpment (30°), from ~32 to 30 km; and depths of 17–20 km under the MV. Moho depths of the profile in an ~ W-E direction at ~31.5°N are from ~30 to 40 km, under topography that increases from 0 to 2,600 m; and became shallower (16 km depth) as the profile reaches the Gulf of California. These results show that deeper Moho is related to higher elevations with an abrupt change under the Main Gulf Escarpment, except for western PRBC where the Moho depth is not simply reflecting isostatic compensation.

1. Introduction

The relative motion between the Pacific and North American plates in the northern Baja California (nBC), Mexico, region is dominated by the transtensional plate boundary that generates normal and strike-slip faults (Stock et al., 1991). This plate boundary generates significant earthquakes in nBC that have reached magnitudes of 7.2 (the 2010 El Mayor-Cucapah earthquake). This significant seismicity is recorded by the Southern California Seismic Network, on the USA side of the border, and by the Northwest Mexico Seismic Network (RESNOM; Centro de Investigación Científica y de Educación Superior de Ensenada, Baja California [CICESE, 1980]), in the nBC region.

Northern Baja California is composed, mainly, of two contrasting geological subregions divided by the Main Gulf Escarpment (MGE; Figure 1): the sedimentary environment of the Mexicali Valley (MV) and the granitic environment of the Peninsular Ranges of Baja California (PRBC). The PRBC is a Mesozoic batholith composed of two belts separated by a magnetite-ilmenite boundary (Gastil et al., 1991): the western batholith with more mafic composition, ages from 140 to 105 Ma, and elevations from 0 to ~900 meters above mean sea level (SL); and the eastern batholith, formed between 105 and 80 Ma, characterized by more silicic intrusions and metasedimentary rocks, with elevations from ~900 to 1980 m in the Sierra Juárez mountain range (around 32°N) and up to 3095 m in the San Pedro Mártir mountain range (~31°N). Active faults within the PRBC include the strike-slip San Miguel-Vallecitos fault system (e.g., Hirabayashi et al., 1996), the strike-slip Tres Hermanos fault system (e.g., Frez et al., 2000) and the strike-slip Agua Blanca fault (e.g., Wetmore et al., 2019). Faults at the eastern boundary of the PRBC include the Sierra Juárez and San Pedro Mártir fault, which has Holocene scarps but does not currently have significant seismicity (Cid-Villegas et al., 2017).

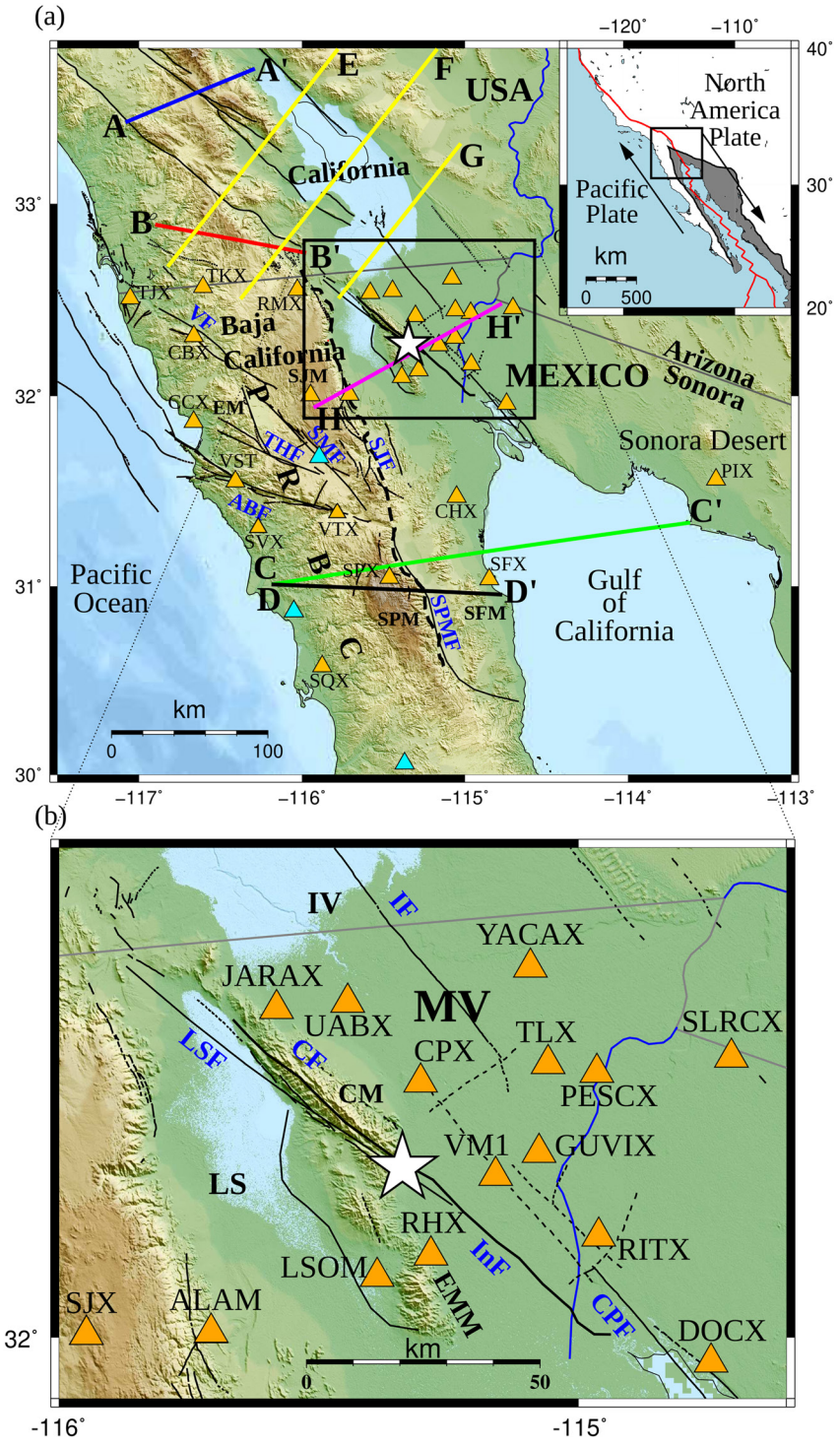
(a)
A
A'
B
B'
C
C'
D
D'
E
F
G
H
H'
USA
California
Baja
California
MEXICO
Arizona
Sonora
Sonora Desert
Pacific
Ocean
Gulf
of
California
North
America
Plate
Pacific
Plate
km
0
500
0
100
TJX
TKX
RMX
CBX
SJM
GCX
EM
VST
PIX
CHX
VTX
SVX
SFX
SPX
SPM
SFM
SQX
VF
THF
SMF
SJF
ABF
SPMF
−120°
−110°
40°
30°
20°
33°
32°
31°
30°
−117°
−116°
−115°
−114°
−113°
(b)
IV
IF
YACAX
JARAX
UABX
MV
TLX
SLRCX
CPX
PESCX
CM
VM1
GUVIX
LS
RHX
RITX
LSOM
SJX
ALAM
DOCX
LSF
CF
InF
EMM
CPF
km
0
50
32°
-116°
-115°

The MV region, the northwestern part of the Gulf Extensional Province (Suárez-Vidal et al., 2008; inset Figure 1), is composed primarily of two major basins divided by the Cucapah and El Mayor mountain ranges: the Mexicali Valley and the Laguna Salada basins (Figure 1). The Laguna Salada Basin is a tectonic depression 20 km wide by 100 km long (García-Abdeslem et al., 2001), and is delimited by the MGE to the west and by the Cucapah and El Mayor mountain ranges to the east. The sedimentation in this basin began when the Cucapah and El Mayor mountain ranges uplifted during the Pleistocene (Martín-Barajas et al., 2001). The Mexicali Valley Basin, located east of the Cucapah and El Mayor mountain ranges, has a depth of 5–6 km and was filled by Neogene sediments transported by the Colorado River (Pelayo et al., 1991). The Cerro Prieto basin is a pull-apart basin within the Mexicali valley controlled by the slip between the Cerro Prieto and Imperial faults (Suárez-Vidal et al., 2008). These faults are considered the main boundary between the North America and Pacific tectonic plates. The Cerro Prieto basin is also identified as a spreading center (Quintanilla-Montoya and Suárez-Vidal, 1996; González et al., 2001). It is a zone of extensional deformation caused by the right lateral movement of the faults mentioned above (Lomnitz et al., 1970). West of the MV (Figure 1b), there is a fault system comprised of the Laguna Salada, Cucapah, and Indiviso faults, the last one is a previously unknown fault that ruptured during the April 4, 2010 M_W 7.2 El Mayor-Cucapah Earthquake (Gonzalez-Ortega et al., 2014). We analyzed the earthquakes in nBC in the time interval 2000 to 2020 (from the RESNOM catalog), by accounting for epicenters inside a polygon that surrounds the above-mentioned faults, and estimate that these two fault systems generate ∼50% of the seismicity in nBC. In the context of the high seismicity of the northern Baja California region, the use of an appropriate velocity structure model, in which the Moho depth is well marked out, will allow improvements in the locations of the earthquakes of the region; by using the proper crustal thickness across the nBC region, e.g., constraining Moho depths of crustal velocity models derived from refraction studies done through the nBC region (Nava & Brune, 1982; Ramirez et al., 2019 and Ramirez-Ramos et al., 2015).

Under this complex tectonic environment, receiver function studies have been carried out to provide a better understanding of the crustal thickness and its relationship with the surface elevation and the extensional processes of the region (Lewis et al., 2001). North of the U.S.A.-Mexico border (southernmost California), in the Mesozoic Peninsular Ranges batholith, Ichinose et al. (1996) and Lewis et al. (2000) performed receiver function studies at latitudes ∼33.5°N and 33°N, respectively (Figure 1). Moho depths proposed by these two authors are similar: 37–36 km at the western part of the batholith to 25–27 km depth at the eastern side of the batholith. Persaud et al. (2007) used receiver functions (RFs) to determine the Moho depth at 17 stations south of 34°N in Southern California, reporting depths from 38 to 25 km. More recently Ozakin and Ben-Zion (2015) analyzed receiver functions at a series of broadband seismometers in southern California in the area from 32.5°N to 34.75°N (profiles E-G, Figure 1) and reported Moho depth ranges from 35 to 40 km (beneath part of the Peninsular Ranges) to 10 km (beneath the Salton Sea).

At present, three studies provide Moho depth estimates based on receiver functions in nBC: those done by Lewis et al. (2001) and Persaud et al. (2007), which used *P*-to-*S* converted phases from teleseismic records; and Reyes et al. (2001), using *Pg*-*Pn* travel times from regional events (Figure 1). These studies used seismic stations from the North Baja Transect installed during 1997 and 1998 at latitude ∼31°N (Astiz et al., 1998). The profile used by Lewis et al. (2001) starts at the Pacific coast, crosses the PRBC, and ends at the Gulf of California coast of Sonora, Mexico, using a station in the Gulf of California itself, while Reyes et al. (2001) used only data from stations in the Peninsular Ranges. Their results for the Moho are similar for the PRBC section, depths of: about 31–33 km near the Pacific coast; 40–42 km beneath the western part of the PRBC; and 19–20 km toward the Gulf of California. These studies have been carried out using profiles that cross

Figure 1. Map of the northern Baja California region. (a) The northern Baja California (Mexico) and southern California (USA) map show the main faults (thin black lines) and the broadband seismic stations used in this study: orange triangles (Electronic Supplement 1). Cyan triangles are the stations used by Persaud et al. (2007) from the NARS-Baja Project (Clayton et al., 2004). The thick straight lines indicate the profiles used in previous receiver function studies: blue, A-A′ (Lewis et al., 2000); red, B-B′ (Ichinose et al., 1996); green, C-C′ (Lewis et al., 2001); black, D-D′ (Reyes et al., 2001); yellow, profiles E-G (Ozakin & Ben-Zion, 2015); pink, H-H′ (Ramírez-Ramos et al., 2015). The thick dashed black line represents the MGE (Martín-Barajas et al., 2001) that divides the Peninsular Ranges of Baja California and the Mexicali Valley (PRBC and MV, respectively). White star indicates the epicenter of the April 4, 2010 El Mayor-Cucapah earthquake. Abbreviations: CM, Cucapah Mountains; EMM, El Mayor Mountains; LS, Laguna Salada; SFM, San Felipe Mountains; SJM, Sierra Juárez Mountains; SPM, San Pedro Mártir Mountains. Fault abbreviations: ABF, Agua Blanca fault; CF, Cucapah fault; CPF, Cerro Prieto fault; IF, Imperial fault; InF, Indiviso fault; LSF, Laguna Salada fault; SJF, Sierra Juárez fault; SMF, San Miguel fault; THF, Tres Hermanos fault; VF, Vallecitos fault. Inset of (a): The interaction between North America and the Pacific plates is shown with black arrows; the gray area shows the Gulf Extensional Province (Suárez-Vidal et al., 2008). (b) Zoomed map of (a) showing details of the MV region with same labels as (a).

the PRBC approximately in a west-east direction with seismic stations installed outside the MV region. Note that Persaud et al. (2007) obtained a Moho depth for three additional sites in the northern PRBC, NE71, NE72 and NE73 (cyan triangles of Figure 1), as part of a regional study using RFs from NARS-Baja seismometers surrounding the Gulf of California (Clayton et al., 2004).

The seismically active region of nBC between ~32°N and 33°N has a gap of receiver function studies. To perform a receiver function study in nBC, we used stations belonging to RESNOM (Figure 1) that were updated from short-period to three-component broadband seismic stations as a consequence of the occurrence of the April 4, 2010 M_W 7.2 El Mayor-Cucapah earthquake (Vidal-Villegas et al., 2018). To increase station coverage in the SW-NE direction (that crosses the PRBC, the MGE, and the MV), we installed temporary broadband stations (Figure 1 and Electronic Supplement 1). Receiver functions from both permanent and temporary stations were calculated using the *P*-to-*S* converted phases from teleseismic earthquakes and then modeled to obtain a Moho depth at each station. Estimating the Moho depth of nBC will provide parameters to characterize the crustal structure related to the PRBC and the MV regions and the tectonic evolution, especially for the MV where the Cerro Prieto Spreading Center is located, as part of the San Andreas-Gulf of California rift system.

2. Data

2.1. Instrumentation

To estimate the Moho depth in nBC, we used 29 broadband seismic stations. These 29 stations comprised of 24 permanent RESNOM stations and five temporary stations (Figure 1 and Electronic Supplement 1). The instrumentation of the permanent seismic stations, at present, includes: two stations with Güralp CMG-40T with Reftek 71A-07 recorder, and CMG-40 TD with Reftek 130 recorder (flat response from 30 and 120 s to 50 Hz, respectively); nine stations equipped with Güralp CMG-3ESPC and Reftek 130 (120 s–50 Hz); 13 stations instrumented with Nanometrics Trillium Compact (NTC) with Reftek 130 (120 s–50 Hz). The temporary seismic stations were instrumented as follows: Four stations with NTC and Nanometrics Taurus (120 s–50 Hz); one station equipped with Geotech KS-2000 and Reftek 130 (120 s–50 Hz).

Ramirez et al. (2019) described the installation facilities of permanent broadband stations. Temporary stations were powered by four deep-cycle batteries (interchangeable every 3 months) and had the following shelters: for stations ALAM, OJSN, and VM1, a concrete base with metal lid was constructed; station VST used a former accelerometer station shelter; station LSOM was buried and covered with plastic boxes under sand over wood. Temporary stations operated differently: ALAM, 3 years; OJSN, 3 years; VM1, 3 years; VST, 1 year; LSOM, 3 months.

2.2. Teleseismic Earthquakes

A preliminary earthquake selection, performed searching in the United States Geological Survey (USGS) Earthquake Catalog (see Data and Resources) for $M \geq 6.5$ earthquakes (from January 1, 2014, to July 1, 2016), resulted in 133 earthquakes. We selected 90 teleseismic earthquakes at epicentral distances between 30° and 95° from the central point of the array at 32.1°N, 115.7°W.

The 90 teleseismic earthquakes, requested from RESNOM (see Data and Resources), were incorporated with records from the temporary stations. Then, we performed two steps of quality control: (i) Checking that the seismic signal was good: Presence of electronic noise due to the absence of seismic signal; (ii) selecting only the events where the *P*-arrival was clear enough above the ambient noise (STA/LTA ratio above 1.5 of the 0.1–1.0 Hz band-pass filtered signal). The seismic ambient noise is higher in stations located in the MV region than in the PRBC (Ramírez et al., 2019, Figure 2 shows this issue). After these steps, 66 teleseismic earthquakes were selected for the receiver function computation (Electronic Supplement 2).

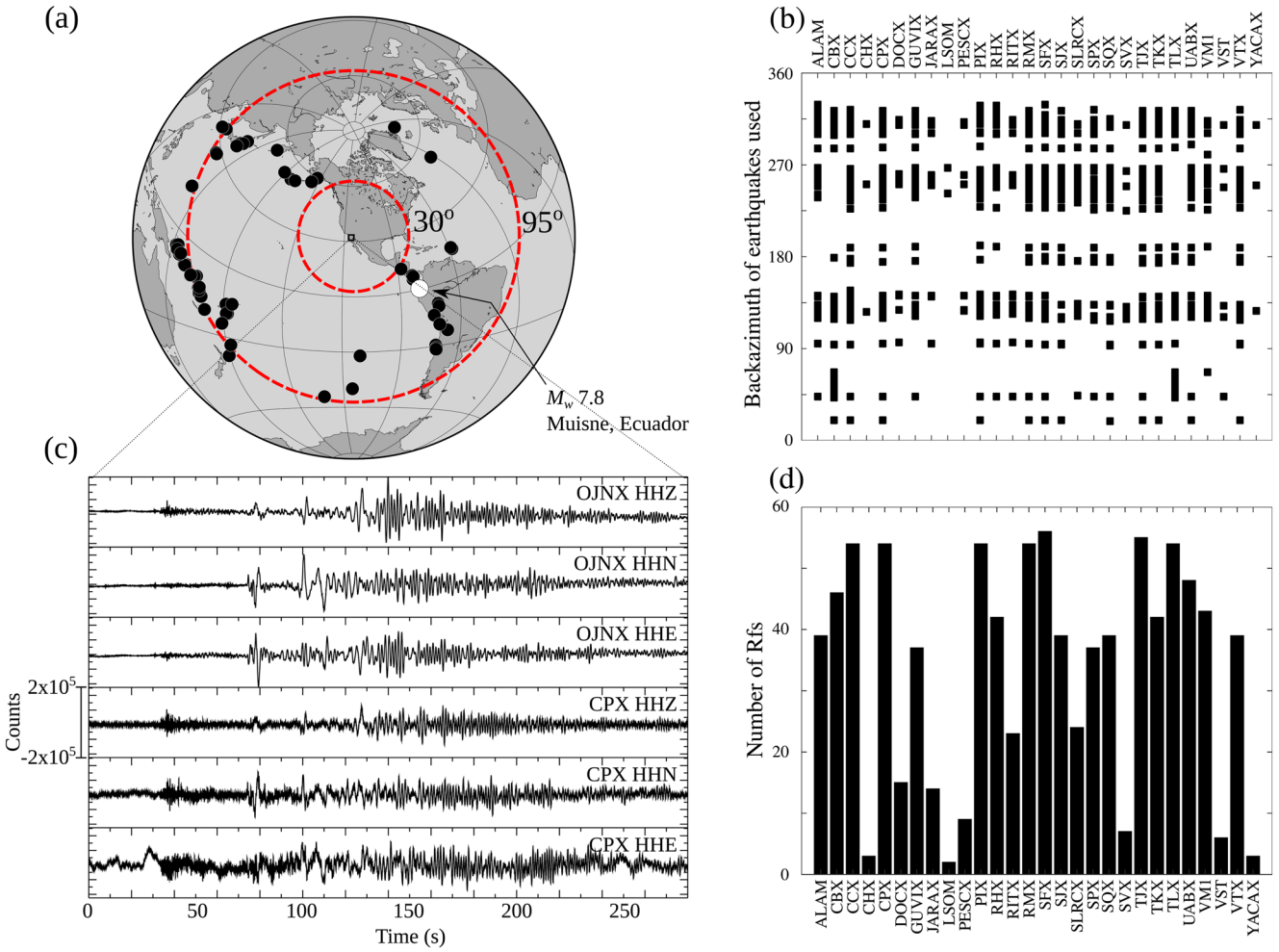

Figure 2. Teleseismic earthquakes used in this study. (a) Global distribution of the earthquakes used (circles filled in black and white). Red dashed lines indicate the 30 and 95° distances from the center of the study area (black rectangle). The white filled circle indicates the position of the April 16, 2016 Muisne, Ecuador earthquake M_w 7.8. (b) Backazimuth distribution of earthquakes used at each station. (c) Three-component raw records of the selected earthquake of stations OJNX and CPX, located in the PRBC and the MV region, respectively. (d) Number of receiver functions calculated at each station. MV, Mexicali Valley; PRBC, Peninsular Ranges of Baja California.

3. Methodology

Moho estimation was performed using the 66 earthquakes selected (Figure 2 and Electronic Supplement 2). In order to compute the RFs of each broadband seismic station in nBC, we first preprocessed the records following these three main steps: (1) Create a SAC-format (Goldstein & Snoke, 2005; see Data and Resources) database following the structure used for data gathering using the Standing Order for Data (Owens et al., 2004); (2) Remove the instrument response of the seismographs using ObsPy (Beyreuther et al., 2010; see Data and Resources) under Spyder (The Scientific Python Development Environment; see Data and Resources), we eliminated the long period noise below 0.05–0.1 Hz, and the high frequency above 10–20 Hz for stations in the PRBC and 10–15 Hz in the MV region, the high corner frequencies used are related to the presence of the seismic noise levels each region: low and high for the PRBC and MV, respectively (Ramirez et al., 2019); (3) Add the theoretical first *P*-wave arrival to the SAC files of each teleseismic earthquake using TauP (see Data and Resources) and visually inspect the arrivals automated picks.

We rotated the north and east components to radial and tangential components (ZRT coordinates). Then a source normalization method is applied, deconvolving the vertical component from the radial component (Figures 3a and 3b). The iterative, time-domain deconvolution to estimate the receiver function was carried

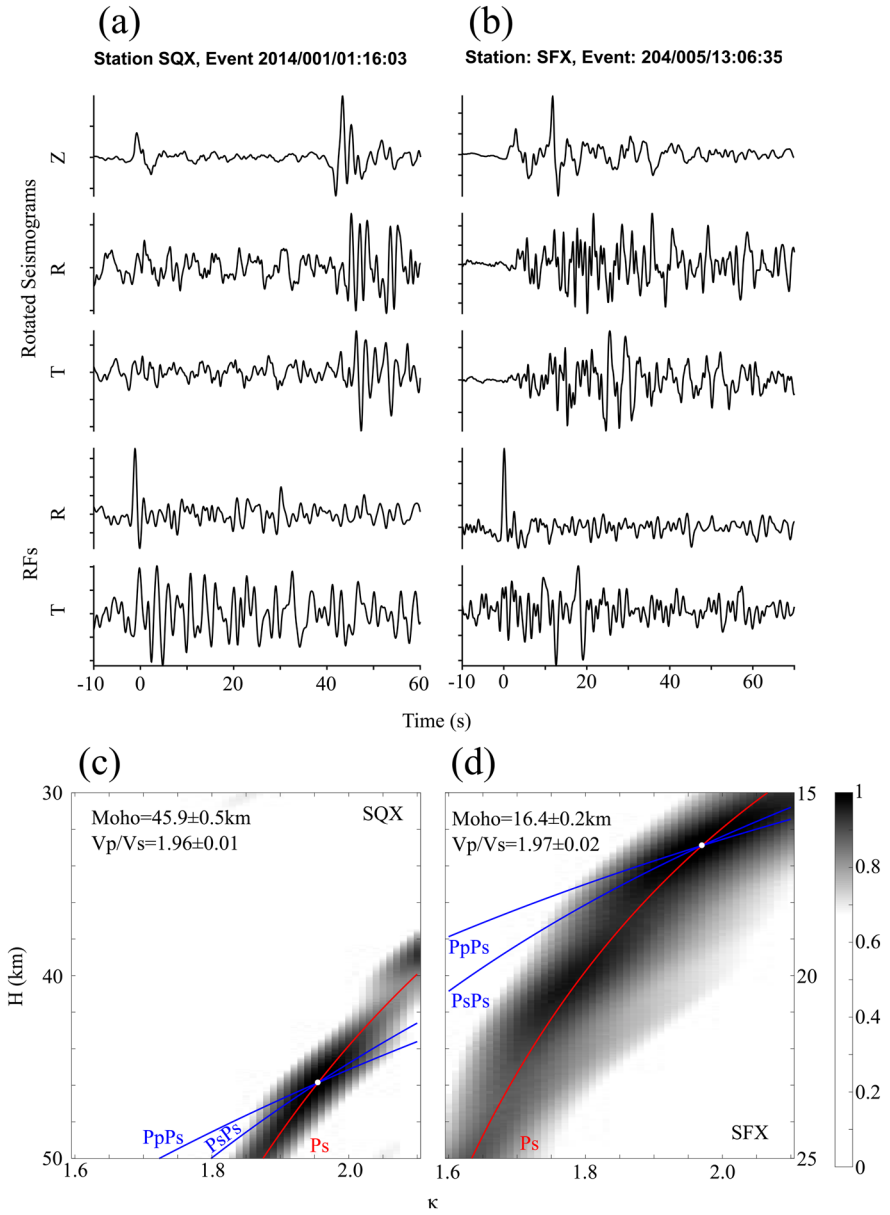

Figure 3. (a) and (b) Data sample for stations SQX and SFX, located in the PRBC and MV regions, respectively. The upper panel shows, from top to bottom, the vertical, radial, and transversal rotated components and the Radial and Transversal components of the RFs. (c) and (d) are the examples of the *H*-κ domain stacking of the stacked receiver functions SQX and SFX, respectively. The white dot marks the maximum determined by 200 bootstrap resamplings of the RFs; the curves represent the phases used in the H-κ stacking process.

out using the code developed by Ligorria and Ammon (1999); the authors tested the technique with data including short and intermediate-period signals, with their share of noisy data.

To estimate the Moho depth, we converted *Ps*-*P* times to depth by using the Matlab toolbox FuncLab (Eagar & Fouch, 2012; Porritt & Miller, 2018). This estimation was obtained using two methods: The FuncLab-implemented Common Conversion Point (CCP; Eagar et al., 2011), and *H*-κ stacking (Zhu et al., 2006; Zhu & Kanamori, 2000). The CCP is a back-projection method where the amplitudes of each receiver function are placed in the respective raypath of the teleseismic earthquake. In this stacking, where the signal is enhanced, the amplitudes and depths are connected based on the position of the ray piercing point. Then the IASP91 (Kennett & Engdahl, 1991) one dimensional velocity model is used to compute the one dimensional

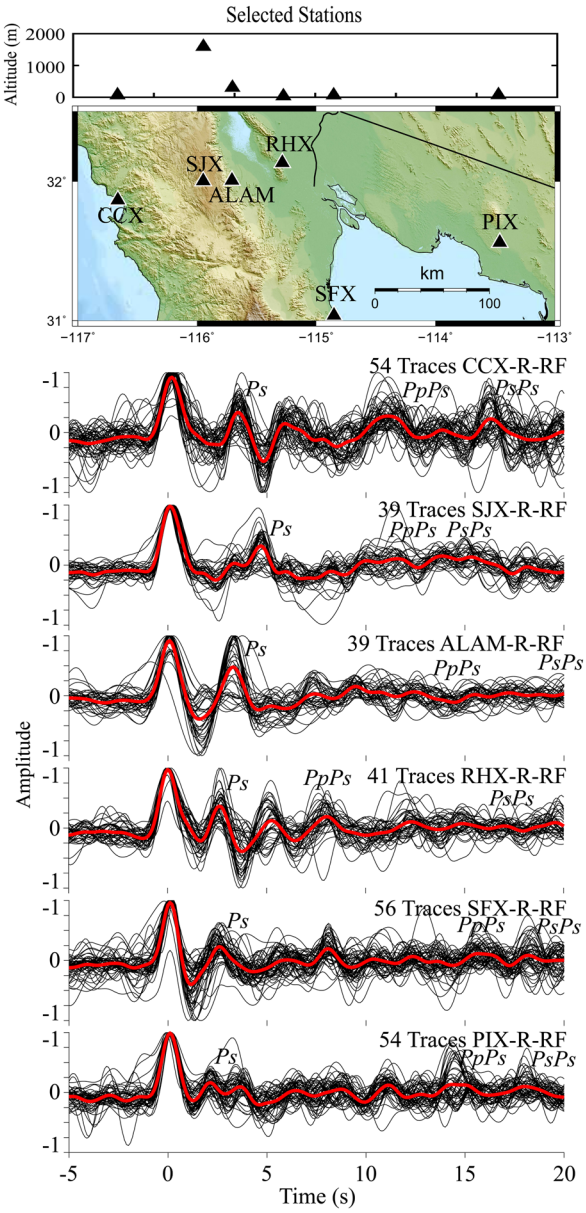

Figure 4. Map of selected stations of nBC and the Sonora Desert and the elevation at each station (top panel). The stacked RFs (thick red lines) of the radial RFs (thin black lines) computed at each of the selected stations are shown in the plots, from station CCX to PIX, from top to bottom, in a west to east direction. The legend at the top-right of each stacked receiver function plot indicates the number of earthquakes used, the station code, and the component code (R-RF; radial RF). The interpreted *Ps* arrivals are indicated at the right-top of the phase. nBC, northern Baja California; RF, Receiver Functions.

ray tracing and the time-to-depth conversion. The starting stacking parameters were: Bootstrap resamples 200 (number of times to resample) and bootstrap percentage of 150 (the percentage of data to resample); minimum and maximum bin width of 0.5° and 2.0°, respectively; minimum and maximum ray parameter of 0.04 and 0.08, respectively; bin spacing of 50 km; maximum depth of 60 km (Figures 3c and 3d).

The *H*-κ stacking is a technique used to determine average crustal properties based on RFs (Zhu & Kanamori, 2000). This method considers a homogeneous, horizontal, and isotropic layer (crust) over a half-space (upper mantle). With the *H*-κ stacking, the Moho depth (*H*), the *P* to *S*-wave velocity ratio (*Vp/Vs* of κ), and the Poisson's ratio are estimated by measuring the *Ps*-*P* time from the RFs. The *H*-κ parameters used for computations were: *Ps*-weight of 0.7, *PpPs*-weight of 0.2, and *PpSs* + *PsPs*-weight of 0.1; κ-min and κ-max of 1.6 and 2.1, respectively; *H* and κ delta of 0.01. Depth range and *Vp* are different for stations located in the PRBC and the MV region: *H*-min = 22.5 km, *H*-max = 45 km, and *Vp* = 6.4 km/s for stations in the PRBC; *H*-min = 15 km, *H*-max = 25 km, and *Vp* = 6.1 km/s for stations in the MV. It is important to mention that for the *H*-κ analysis, we did not separate stations deployed in the MV basin for the Moho estimations.

4. Results

4.1. Receiver Functions of nBC

The RFs were computed from 66 earthquakes, with good azimuthal coverage, especially along the Peru-Chile Trench; in the Tonga-Hikurangi Trench, from the Solomon Sea to New Zealand; and in the Aleutian Trench, from the Gulf of Alaska to Japan (Figure 2).

The stacked RFs of the PRBC show the *Ps* conversion around 4.1 s. As examples, we selected stations CCX, and SJX, located at the Pacific Coast and at the eastern side of the PRBC (top of the MGE), respectively. For the MV region, we identified the *Ps* conversions around 2.0 s. As examples, we show RFs stacks for stations ALAM, RHX, SFX, and PIX (Figure 4), located at the eastern base of the PRBC (at the bottom of the MGE, inside Laguna Salada), in the Mexicali Basin (east of El Mayor Mountain), at the Gulf of California coast, and in the Sonora Desert (now in the North American Plate), respectively. In Electronic Supplement 3 are all the rotated seismograms used in the analysis of all the stations and the corresponding RFs.

4.2. Back-Projection Receiver Functions

The back-projection results of the RFs were manually selected from the maxima of the most coherent phase from three profiles (Figure 5a): A1-A1′, from the PRBC, crossing the MGE into the MV; A2-A2′, which crosses the BC peninsula, around San Pedro Mártir mountain, and ends at the Sonora desert; A3-A3′, an almost N-S profile that runs through the PRBC. The A1-A1′ profile (upper panel of Figure 5b) presents positive RFs with high amplitudes (RF ray parameter amplitudes of ∼0.1) at depths of around 30 km, for stations close to the Pacific coast of the peninsula (CCX, VST, and CBX); from 30 to 42 km for stations located around the Sierra Juárez mountains (VTX and SJX); 25–30 km for stations located in the transition segment between the PRBC and MV (ALAM and RMX); 17–25 km for stations located in the MV region (JARAX–SLRX). The back-projected RF ray parameter amplitudes of the A3-A3′ profile present positive high values (amplitudes of ∼0.1) at the following depths

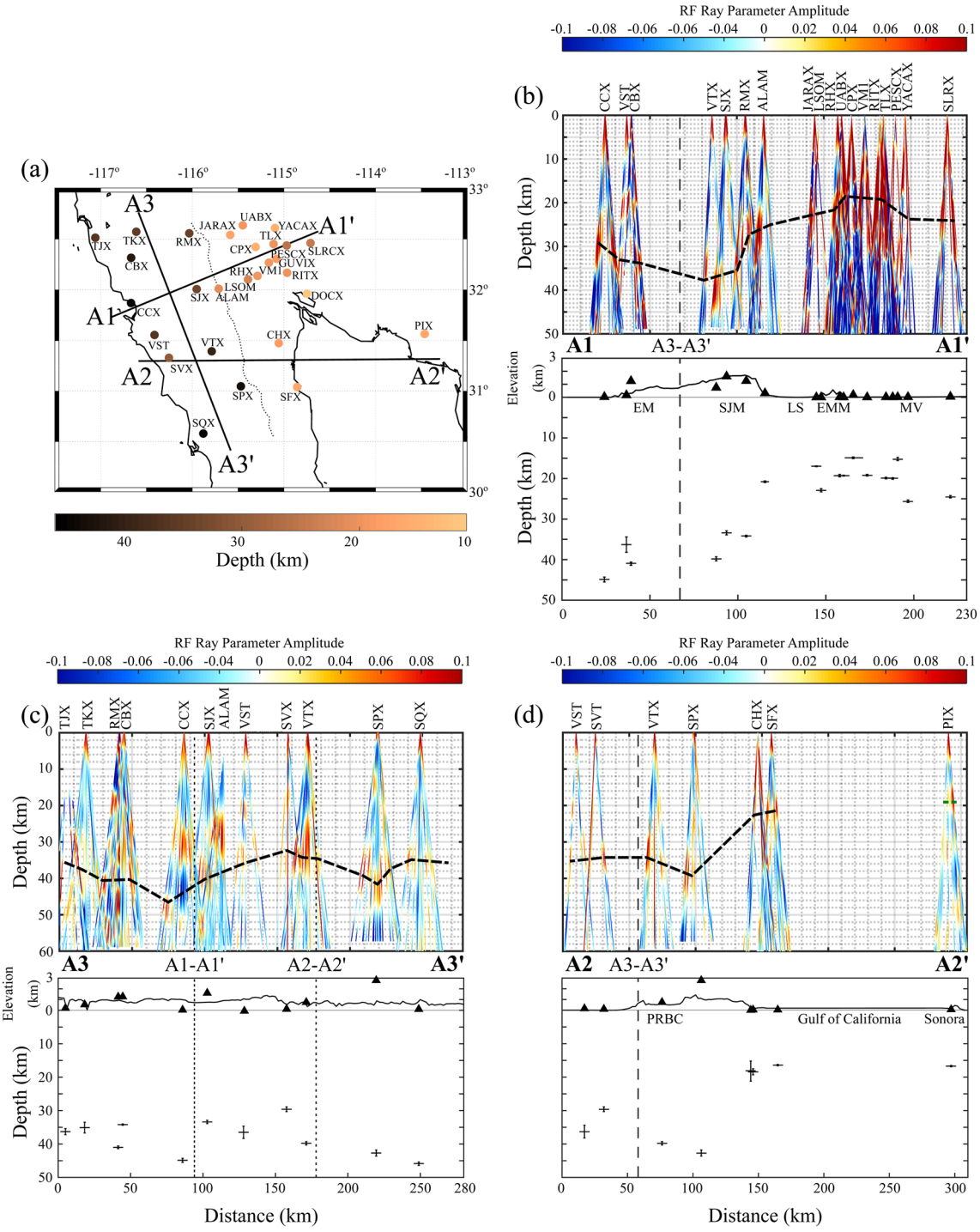

Figure 5. (a) Map of estimated depths from the *H*-κ analysis at each seismic station. Black thick lines indicate the analyzed profiles. The thin dotted line indicates the MGE (Martín-Barajas et al., 2001). Plots (b), (c), and (d) show the back-projected RFs ray parameter amplitude of the profiles A1-A1′, A2-A2′, and A3-A3′, respectively; the dashed thick black line indicates the suggested Moho from the interpreted ray paths. The lower figure in panel (b), (c), and (d) of the A1-A1′, A2-A2′, and A2-A2′, respectively, shows: the results of Moho depth estimation with error bars from the *H*-κ procedure (Table 1); the elevation calculated along each profile, black line; mean sea level, thin black line; location of each station alongside the profile, black triangles; the location at which the A3-A3′ crosses the profile, dashed line; the location at which A1-A1′ and A2-A2′ cross the profile, dotted lines. MGE, Main Gulf Escarpment.

Table 1
Receiver Function Results and Moho Estimations of Each Station

Station code	Elevation (m)	RFs used	*Ps-P* time (s)	*H* (km)	V_P/V_S, κ	Poisson's ratio
ALAM	315	39	3.2	20.8 ± 0.2	1.84 ± 0.02	0.292 ± 0.005
CBX	1,250	46	4.5	41.0 ± 0.4	1.96 ± 0.01	0.324 ± 0.004
CCX	33	54	3.6	44.9 ± 0.6	1.97 ± 0.02	0.327 ± 0.004
CHX	49	3	2.5	18.4 ± 0.9	1.74 ± 0.06	0.252 ± 0.024
CPX	179	54	3.2	14.9 ± 0.2	1.95 ± 0.02	0.321 ± 0.005
DOCX	13	15	1.4	10.9 ± 0.2	1.95 ± 0.03	0.208 ± 0.015
GUVIX	14	37	3.3	18.2 ± 3.0	1.87 ± 0.10	0.299 ± 0.026
JARAX	5	14	2.5	17.0 ± 0.1	1.85 ± 0.01	0.292 ± 0.004
LSOM	5	2		22.9 ± 0.4	1.55 ± 0.02	0.140 ± 0.012
PESCX	23	9	1.8	25.6 ± 0.3	1.72 ± 0.01	0.246 ± 0.005
PIX	72	54	2.2	16.7 ± 0.2	1.81 ± 0.02	0.280 ± 0.005
RHX	16	42	2.5	19.3 ± 0.3	1.75 ± 0.02	0.260 ± 0.008
RITX	14	23	1.8	20.0 ± 0.2	1.54 ± 0.01	0.137 ± 0.008
RMX	1,265	54	4.7	34.2 ± 0.2	1.61 ± 0.01	0.186 ± 0.005
SFX	48	56	2.6	16.4 ± 0.2	1.97 ± 0.02	0.327 ± 0.004
SJX	1,609	39	4.8	33.4 ± 0.5	1.57 ± 0.01	0.158 ± 0.008
SLRCX	49	24	1.2	24.5 ± 0.3	1.75 ± 0.02	0.256 ± 0.008
SPX	2790	37	4.9	42.7 ± 0.9	2.04 ± 0.03	0.341 ± 0.006
SQX	101	39	3.4	45.9 ± 0.5	1.96 ± 0.01	0.323 ± 0.003
SVX	111	7	4.1	29.6 ± 0.7	1.82 ± 0.03	0.282 ± 0.010
TJX	198	55	3.9	36.3 ± 0.9	1.62 ± 0.02	0.194 ± 0.012
TKX	535	42	3.3	35.1 ± 1.6	1.90 ± 0.04	0.309 ± 0.011
TLX	17	54	2.0	19.9 ± 0.2	1.95 ± 0.02	0.321 ± 0.004
UABX	5	48	3.5	19.3 ± 0.1	1.49 ± 0.01	0.090 ± 0.001
VM1	10	43	2.2	19.2 ± 0.2	1.64 ± 0.02	0.204 ± 0.009
VST	163	6	3.7	36.3 ± 1.9	1.65 ± 0.04	0.209 ± 0.0.21
VTX	746	39	4.1	39.8 ± 0.5	1.92 ± 0.02	0.315 ± 0.005
YACAX	21	3	1.9	15.2 ± 0.4	2.06 ± 0.04	0.346 ± 0.008

(upper panel of Figure 5c): 35–42 km for stations south 31°N (SPX and SQX); 32–46 km for stations located between 31°N and 32°N (VTX, SVX, VTS, and SJX; except for stations ALAM and CCX located at the east and west limits of the PRBC, respectively, at around sea level); and 35–40 km for stations between 32°N and 33°N (CBX, RMX, TKX, and TJX). The amplitudes of the back-projected RFs ray parameters of the A2-A2' profile (upper panel of Figure 5d) present high positive values at depths of ~35 km for stations located near the Pacific coast (VST and SVT); 35–40 km for stations around the San Pedro Mártir mountains (VTX and SPX); ~23 km for stations near the Gulf of California coast (CHX and SFX); and ~20 km for the station located in the Sonora Desert (PIX).

4.3. *H-κ* Computations

The results of computations from the *H-κ* analysis (Figures 3c and 3d) are shown in Table 1 and Figure 5 (divided into the three profiles). From this analysis we estimate a Moho depth of ~38 km, for stations deployed in the PRBC, and ~19 km, for stations located in the MV region (Table 1). Like in the back-projection analysis, results of Moho depth from the *H-κ* computation (Table 1) are analyzed in the same A-A' profiles. Stations projected into the A1-A1' profile (lower panel of Figure 5b) show that Moho depths under stations

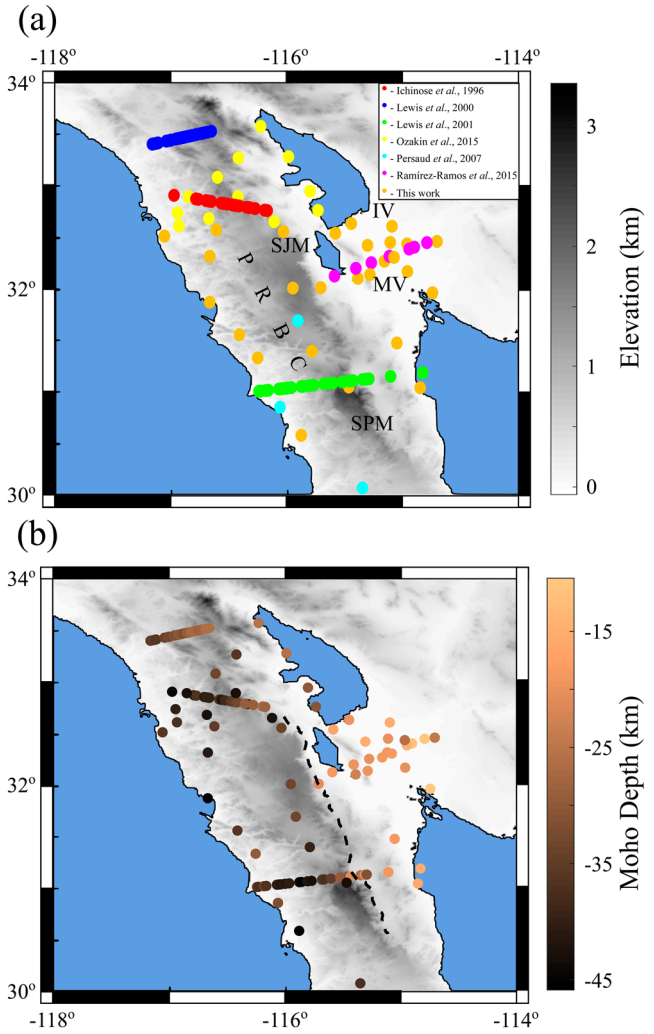

Figure 6. Moho dephts for northern Baja California. (a) Local topography, main geological regions, color dots represent the Moho estimations of the regional studies indicated in the upper right-handed legend box. (b) Moho estimations by seismic studies in northern Baja California; Colorbars to the right of the maps indicate elevation and Moho depth Black dashed line in (b) represents the MGE (Martín-Barajas et al., 2001). MGE, Main Gulf Escarpment.

located on the Pacific coast of the Peninsula (CCX, VST, and CBX) vary from 35 to 45 km. Moho depths from stations deployed in the Sierra Juárez mountains region (VTX, SJX, and RMX) range from 35 to 40 km. The Moho depths of stations in the MV region range from 15 to 25 km. The A3-A3′ profile (lower panel of Figure 5c) has the following Moho depths: From ∼35 km dipping to a maximum of 45 km, in the north-south direction, for profile section from 33°N to 32°N; from ∼32 km dipping into 46 km depth, in the north-south direction, for the profile section between latitudes 32°N and ∼30.5°N. The profile A2-A2′ (lower panel of Figure 5d) presents Moho depths of (Table 1): About ∼30 and 36 km for stations near the Pacific coast (SVT and VST); 40–42 km for stations at the center of the Peninsula (VTX and SPX); 16–19 km for stations near the Gulf of California (SFX and CHX); and ∼17 km for the station located in Sonora, Mexico (PIX). All of the *H-κ* stackings for all the analyzed stations are shown in the Electronic Supplement 3.

Moho depths from previous studies (Ichinose et al., 1996; Lewis et al., 2000, 2001; Ozakin and Ben-Zion, 2015; Persaud et al., 2007; Ramírez-Ramos et al., 2015) were compared to the results from our *H-κ* computations. The interpretation of Moho in northern Baja California, alongside the topography, is shown in Figure 6.

5. Analysis

These results now allow us to examine the variations of the Mojo depth across the region and how these are related to the regional geology and tectonic provinces of northern Baja California and the Pacific-North America plate boundary. Recall that we have two different types of results for each station because of the two different methods used. In general, results from the back-projection of the RFs are similar to those resulting from the *H-κ* computations (Figures 5b–5d). We discuss the Moho depth analysis using the results from the *H-κ* computations. The individual site results from the profiles in Figure 5, as well as previously published values, are colored in Moho depth to show how the Moho depth varies in map view (Figure 6).

Along the A1-A1′ profile (Figures 5a and 5b), shows that the Moho depth become shallower eastward, starting at 45 km depth at the western part of the profile, reaching ∼34 km depth below stations near the top of the MGE, following the high elevations of the Sierra Juárez mountain range. The deepest Moho depths are at the Pacific coast. Thus, the Moho depth is not simply reflecting isostatic compensation of the batholith. The Moho depth changes abruptly when the profile enters the MV region: from ∼32 km below the PRBC to a 20 km depth at the lower part of the MGE (at Laguna Salada basin). This abrupt change is quite steep (∼30°dip) but it does not correlate with the strongest topographic gradient. Rather, it is most tightly constrained in map view between stations SJX and ALMX (aligned in the profile A1-A1′ and separated ∼22 km; Figure 5a), west of the Main Gulf Escarpment. This local dip represents an uncertainty of ∼2.5 km for a 35 km-thick crust, representing ∼7% of the total crustal thickness; close to the ∼2 km and 6% for a 30 km-thick crust estimated by Lewis et al. (2001). Like the results from Lewis et al. (2001), we can say that, in general, the Moho results are not affected much by the shifts of the projection points in a dipping Moho.

Continuing eastward along profile A1-A1′, the Moho depths for the MV region section of the A1-A1′ profile are shallow, and stable at ∼20 km depth. Comparing the Moho depths of the MV with those reported by Ramírez-Ramos et al. (2015), in a refraction profile (using *Pn* arrivals) that ran in the same position (A1-A1′), we get similar results. For the Laguna Salada basin, we get ∼20 km Moho depth, while the authors

reported 19 km depth. Moreover, for the MV basin, we get ~17 km Moho depth, while they reported 15 km. This ~2 km difference may be because Ramirez-Ramos et al. (2015) did not have a reverse blast, and therefore coverage rays, for modeling the Laguna Salada region.

The almost N-S profile (A3-A3′) runs entirely through the PRBC, which is a tectonically stable topographic region whose elevations start at sea level at the Pacific coast, and reach 2,600 m SL at the top of the MGE. The elevations along the profile A3-A3′ are generally about 1 km, so this profile is west of, although roughly parallel to, the ~2.5 km elevation of the crest of the mountain range. Nevertheless, Moho depths show some variations in a N-S direction: From 33° to 32°N, the Moho deepens from 35 to 45 km; from 32°N to 30.5°N the Moho deepens from ~30 to 46 km. The mean Moho depth for the PRBC (~38 km) is close to the 42 km reported by Nava and Brune (1982). This model consists of a flat-layer model for the PRBC derived from a refraction profile that ran almost in the same position as A3-A3′. The Moho depth in the PRBC, at a single station at 31.7°N, was determined to be 33.7 km (Persaud et al., 2007), consistent with the results we found here.

The Moho depths for the A2-A2′ profile first increase eastward and then decrease, similar to changes in the elevation profile (lower panel of Figure 5d). From west to east, the Moho deepens as elevation reaches its maximum (2,600 m SL; station SPX): from ~30 to 42 km depth. Continuing eastward, as elevation decreases going into the Gulf of California, the Moho goes from 42 to 16 km depth, almost the same as the depth below PIX located in the Sonora Desert. The Moho depths reported by Lewis et al. (2001) from the receiver function profile (Figure 1) present the same behavior and values as those from the A2-A2′ profile, 55 km south of C-C′ profile (Lewis et al., 2001, Figure 1).

Our results can be compared to the RF results from southernmost California reported by Ozakin and Ben-Zion (2015), even though our data are from northwestern Mexico, just south of the SW end of their profiles E, F, and G (Figure 1). Ozakin and Ben-Zion (2015) noted that the depth to the Moho varied along strike in a complex fashion, which is also characteristic of our results. For example, in our profile A3-A3′, parallel to the axis of the Peninsular Ranges, the Moho depths vary generally in the range from 35 to 45 km but without any systematic direction of gradient. The Moho depths >40 km are beneath the Peninsular Ranges in two locations 150 km apart at latitudes between 30.5°N and 32°N. In combination with the Moho depths reaching 40 km reported by Ozakin and Ben-Zion at 34°N beneath the batholith, this suggests a N-S variation in Moho depth under the batholith, with a wavelength of 150–200 km. We note that such variations in Moho depth are also known from the next regional batholith to the north (the Sierra Nevada batholith in central California). There, the Moho depths defined by *PmP* reflections vary from <34 km to >40 km along a 350 km long strike line (Fliedner et al., 2000) although the along-strike variations there are irregularly spaced and in some cases shorter in wavelength than the ones we can resolve in the PRBC.

Another important regional question is the crustal thickness and thickness variations in the plate boundary zone in the Mexicali Valley. The Moho depths in the MV in our study area are in the range of 15–20 km. Because of the good station density, we have a high confidence in this result. These are consistent with the Moho depths determined from *PmP* reflections along an active-source line in the Imperial Valley, where the shallowest Moho identified was 17 km depth (Han et al., 2016) beneath the Brawley Seismic Zone. Note, however, at our easternmost station in the Mexicali Valley the Moho depth approaches 25 km (SLRCX, Figure 5a).

We only identify one station (DOCX, Table 1) with Moho depth nearly as shallow as the ~10 km depth suggested by Ozakin and Ben-Zion (2015) for the Moho beneath and east of the Salton Sea. This station is in Sonora, just E of the southern extension of the Cerro Prieto Fault, where it enters the northern Gulf of California (Figure 1) and its Moho depth by *H-k* analysis is 10.9 ± 0.2 km. Ozakin and Ben-Zion (2015) used receiver functions from a broadband seismic network in California to identify offsets (steps) in the Moho along the traces of some of the active faults. Our available seismic network was much less dense, so that identifications of such offsets are more uncertain. However, the unusually shallow depth to the Moho seen at DOCX may represent a possible abrupt Moho topography or a step offset due to proximity to the Cerro Prieto fault (depending on the dip angle) over the narrow region of the San Andreas-Gulf of California rift system (Figure 1).

Han et al. (2016) identified a reflector at about 20 km depth on an active-source seismic line that extended southeastward from the Imperial Valley to the eastern Mexicali Valley. Their data showed that this reflector is the Moho in the Imperial Valley, but using observations of refracted arrivals they hypothesize that this reflector continues laterally to a mid-crustal reflector below which the Moho deepens from 20 to 30 km depth for a short distance along the line. This observation might be consistent with the fact that we see a slightly larger Moho depth at SRLCX compared to the stations to the west of it, in the Mexicali Valley.

Figure 6 shows the integrated Moho structure from the northern Peninsular Ranges, California to the southern PRBC and Salton Trough Province (STP), from all seismic exploration studies performed in the region (Ichinose et al., 1996; Lewis et al., 2000, 2001; Ozakin and Ben-Zion, 2015; Persaud et al., 2007; Ramírez-Ramos et al., 2015; and this study). From that figure, it is clear that the Moho depth in STP is shallower than in PRBC. There is a correlation between the topography in the PRBC region and Moho depth variation: High elevations correspond to deep values, giving support to the Airy theory. Regarding the STP, where Mexicali Valley is located, the figures show a depth of Moho of around 17 km with no marked variations (smooth Moho).

6. Conclusions

In a profile that crosses the PRBC and the MV region, Moho depths became shallower from west to east: 45 to ~34 km under the PRBC to 17 km under the MV region; with an abrupt change in depth under the MGE, from ~32 to 20 km depth in a west to east direction. Moreover, under the MV region, we propose a near-constant Moho depth of 17–20 km. Along the profile that runs almost N-S though the PRBC, with stable topography, Moho depths vary from 35 to 45 km, from 33°N and 32°N; and from 30 to 46 km depth from 32°N to 30.5°N. The Moho depths, in a profile aligned in an almost E-W direction (at ~31.3°N), follow the altitude of the topography from 0 to 2,600 m SL: from ~30 to 40 km depth.

The Moho becomes shallower as the profile reaches the Gulf of California coast to a 16 km depth in both the Peninsula of Baja California and in the station located on the coast of Sonora. Our results are similar to previous studies done north and south of the study region (Han et al., 2016; Lewis et al., 2001; Ozakin & Ben-Zion, 2015; Persaud et al., 2007), and with refraction studies done in profiles that ran close to the ones here reported (Nava & Brune, 1982; Ramírez-Ramos et al., 2015). The results of our study show that, in general, the Moho depth follows the elevations of the stations, deeper for stations with high altitudes and shallower for stations near sea level, with an abrupt change in depth at the surrounding area of the Main Gulf Escarpment. The Moho depths at stations in the MV region are shallow, suggesting an extension of the lower crust of the pull-apart basin that connects the Cerro Prieto and Imperial faults (Cerro Prieto Spreading Center), within the regional section of the rifting system San Andreas-Gulf of California.

Acknowledgments
Part of the financial support for this project was provided by CONACYT (CB-2009-133019 SEP-CONACYT). The first author worked under the Scholarship Number 254218 granted by the National Council of Science and Technology of Mexico (CONACYT), the CONACYT 2018 Foreign Mobility Fellowship (291250), and by the Mobility Fellowship granted by the Autonomous University of Baja California: research residence (announcement 76). The comments and suggestions provided by Christian Stanciu and the anonymous reviewer substantially improved the content of this article. Alejandra Núñez-Leal facilitated teleseismic data streams from the local seismic network (RESNOM). For the installation and service for the seismic stations, the authors acknowledge Oscar Gálvez, Luis Orozco, and Ignacio Méndez, from the Earth Sciences Division of CICESE. Sergio Arregui provided the main script used for creating the maps in Generic Mapping Tools. J. Antonio Vidal-Villegas dedicates this article to the memory of Luis R. Orozco León (1951-2021), for many years the engineer in charge of maintenence the RESNOM stations.

Data Availability Statement

Raw and processed seismic signals, as well as the poles and zeros of stations and main scripts used can be found in https://zenodo.org/record/4017974#.X1Z_SHkzaUl (https://doi.org/10.5281/zenodo.4017974). Teleseismic catalog was obtained from the USGS Earthquake Catalog, available at https://earthquake.usgs.gov/earthquakes/search/ (last accessed September 2020). Data from the Northwest Mexico Seismic Network are available, since September 10, 2014, from the Incorporated Research Institutions for Seismology Data Management Center (IRIS-DMC) at http://ds.iris.edu/mda/BC (last accessed September 2020). The teleseismic data used in this study and the stations Dataless are available upon request to M. Alejandra Nuñez-Leal (anunez@cicese.mx). The *P*-wave travel times were computed, and added to earthquakes data with TauP. The FuncLab toolbox used for estimating the Moho depth is available at https://robporritt.wordpress.com/software/ (last accessed September 2020). Some plots were made using the Generic Mapping Tools.

References

Astiz, L., Castro, R., Eakins, J., Vernon, F. L., Rebollar, C., Day, S. M., & Brune, J. N. (1998). The North Baja Transect (NBT): A seismic experiment in our backyard. Paper Presented at 10th Annual IRIS Workshop.

Beyreuther, M., Barsch, R., Krischer, L., Megies, T., Behr, Y., & Wassermann, J. (2010). ObsPy: A Python Toolbox for Seismology. *Seismological Research Letters*, *81*(3), 530–533. https://doi.org/10.1785/gssrl.81.3.530

Centro de Investigación Científica y de Educación Superior de Ensenada (CICESE) Ensenada Baja California, México. (1980). Red Sísmica del Noroeste de México. https://doi.org/10.7914/SN/BC

Cid-Villegas, G., Mendoza, C., & Ferrari, L. (2017). Mexico Quaternary Fault Database. *Terra Digitalis*, *1*(1), 1–9. https://doi.org/10.22201/igg.terradigitalis.2017.1.3.50

Clayton, R. W., Trampert, J., Rebollar, C., Ritsema, J., Persaud, P., Paulssen, H., et al. (2004). The NARS-Baja seismic array in the Gulf of California rift zone. *Margins Newsletter*, *13*, 1–4.

Eagar, K. C., & Fouch, M. J. (2012). FuncLab: A MATLAB interactive toolbox for handling receiver function datasets. *Seismological Research Letters*, *83*(3), 596–603. https://doi.org/10.1785/gssrl.83.3.596

Eagar, K. C., Fouch, M. J., James, D. E., & Carlson, R. W. (2011). Crustal structure beneath the High Lava Plains of eastern Oregon and surrounding regions from receiver function analysis. *Journal of Geophysical Research*, *116*. https://doi.org/10.1029/2010JB007795

Fliedner, M. M., Klemperer, S. L., & Christensen, N. I. (2000). Three-dimensional seismic model of the Sierra Nevada arc, California, and its implications for crustal and upper mantle composition. *Journal of Geophysical Research: Solid Earth*, *105*(B5), 10899–10921. https://doi.org/10.1029/2000JB900029

Frez, J., González, J. J., Acosta, J. G., Nava, F. A., Méndez, I., Carlos, J., et al. (2000). A Detailed Microseismicity Study and Current Stress Regime in the Peninsular Ranges of Northern Baja California, Mexico: The Ojos Negros Region. *Bulletin of the Seismological Society of America*, *90*(5), 1133–1142. https://doi.org/10.1785/0119990164

García-Abdeslem, J., Espinoza-Cardeña, J. M., Munguía-Orozco, L., Wong-Ortega, V. M., & Ramírez-Hernández, J. (2001). Crustal structure from 2-D gravity and magnetic data modeling, magnetic power spectrum inversion, and seismotectonics in the Laguna Salada basin, northern Baja California, Mexico. *Geofisica Internacional*, *40*(2), 67–85. https://doi.org/10.22201/igeof.00167169p.2001.40.2.370

Gastil, R. G., Kimbrough, J., Tainosho, Y., Shimizu, M., & Gunn, S. (1991). Plutons of the eastern Peninsular Ranges, southern California, USA and Baja California, Mexico. In *Geological excursions in southern California and México: San Diego, California* (pp. 319–331). Geological Society Of America Annual Meeting Guidebook.

Goldstein, P., & Snoke, A. (2005). "SAC Availability for the IRIS Community". *Incorporated Institutions for Seismology Data Management Center Electronic Newsletter*, *7*.

González, M., Munguía, L., Vidal, A., Wong, V., González, M., & Suárez, F. (2001). Two Mw 4.8 Cerro Prieto, Baja California, Mexico, Earthquakes on 1 June and 10 September 1999: Strong-Motion Observations. *Bulletin of the Seismological Society of America*, *91*(6), 1456–1470. https://doi.org/10.1785/0120000033

Gonzalez-Ortega, A., Fialko, Y., Sandwell, D., Alejandro Nava-Pichardo, F., Fletcher, J., Gonzalez-Garcia, J., et al. (2014). El Mayor-Cucapah (Mw7.2) earthquake: Early near-field postseismic deformation from InSAR and GPS observations. *Journal of Geophysical Research: Solid Earth*, *119*(2), 1482–1497. https://doi.org/10.1002/2013JB010193

Han, L., Hole, J. A., Stock, J. M., Fuis, G. S., Kell, A., Driscoll, N. W., et al. (2016). Continental rupture and the creation of new crust in the Salton Trough rift, Southern California and northern Mexico: Results from the Salton Seismic Imaging Project. *Journal of Geophysical Research: Solid Earth*, *121*, 7469–7489. https://doi.org/10.1002/2016JB013139

Hirabayashi, C. K., Rockwell, T. K., Wesnousky, S. G., Stirling, M. W., & Suarez-Vidal, F. (1996). A neotectonic Study of the San Miguel-Vallecitos fault, Baja California. *Bulletin of the Seismological Society of America*, *86*(6), 1770–1783.

Ichinose, G., Day, S., Magistrale, H., Prush, T., Vernon, F., & Edelman, A. (1996). Crustal thickness variations beneath the Peninsular Ranges, southern California. *Geophysical Research Letters*, *23*(22), 3095–3098. https://doi.org/10.1029/96GL03020

Kennett, B. L. N., & Engdahl, E. R. (1991). Traveltimes for global earthquake location and phase identification. *Geophysical Journal International*, *105*(2), 429–465. https://doi.org/10.1111/j.1365-246X.1991.tb06724.x

Lewis, J. L., Day, S. M., Magistrale, H., Castro, R. R., Astiz, L., Eakins, J., et al. (2001). Crustal thickness of the peninsular ranges and gulf extensional province in the Californias. *Journal of Geophysical Research*, *106*(B7), 13599–13611. https://doi.org/10.1029/2001JB000178

Lewis, J. L., Day, S. M., Magistrale, H., Eakins, J., & Vernon, F. (2000). Regional crustal thickness variations of the Peninsular Ranges, southern California. *Geology*, *28*(4), 303–306. https://doi.org/10.1130/0091-7613(2000)28<303:RCTVOT>2.0.CO;2

Ligorria, J. P., & Ammon, C. J. (1999). Iterative deconvolution and receiver-function estimation. *Bulletin of the Seismological Society of America*, *89*, 1395–1400.

Lomnitz, C., Mooser, F., Allen, C. R., Brune, J. N., & Thatcher, W. (1970). Seismicity and tectonics of the northern Gulf of California region, México: Preliminary results. *Geofisica Internacional*, *10*, 37–48.

Martín-Barajas, A., Vázquez-Hernández, S., Carreño, A. L., Helenes, J., Suárez-Vidal, F., & Alvarado-Rosales, J. (2001). Late Neogene stratigraphy and tectonic control on facies evolution in the Laguna Salada basin, northern Baja California, Mexico. *Sedimentary Geology*, *144*, 5–35. https://doi.org/10.1016/S0037-0738(01)00133-6

Nava, F. A., & Brune, J. N. (1982). An earthquake-explosion reversed refraction line in the Peninsular Ranges of southern California and Baja California Norte. *Bulletin of the Seismological Society of America*, *72*(4), 1195–1206.

Owens, T. J., Crotwell, H. P., Groves, C., & Oliver-Paul, P. (2004). SOD: Standing order for data. *Seismological Research Letters*, *75*(4), 515–520. https://doi.org/10.1785/gssrl.75.4.515-a

Ozakin, Y., & Ben-Zion, Y. (2015). Systematic receiver function analysis of the Moho geometry in the Southern California plate-boundary region. *Pure and Applied Geophysics*, *172*(5), 1167–1184. https://doi.org/10.1007/s00024-014-0924-6

Pelayo, A., Razo, L. A., Gutiérrez, N. L. C. A., Arellano, G. F., Espinoza, J. M., & Quijano, J. L. (1991). Main geothermal fields of Mexico: Cerro Prieto geothermal field, Baja California. *Geological Society of America, The Geology of North America, Economic Geology, México, Guillermo P. Salas. P-3*, 23–58.

Persaud, P., Pérez-Campos, X., & Clayton, R. W. (2007). Crustal thickness variations in the margins of the Gulf of California from receiver functions. *Geophysical Journal International*, *170*(2), 687–699. https://doi.org/10.1111/j.1365-246X.2007.03412.x

Porritt, R. W., & Miller, M. S. (2018). Updates to FuncLab, a Matlab based GUI for handling receiver functions. *Computers & Geosciences*, *111*, 260–271. https://doi.org/10.1016/j.cageo.2017.11.022

Quintanilla-Montoya, A. L., & Suárez-Vidal, F. (1996). Cerro Prieto and its relation to the Gulf of California spreading centers. *Ciencias Marinas*, *22*(1), 91–110. https://doi.org/10.7773/cm.v22i1.832

Ramírez, E. E., Antonio Vidal-Villegas, J., Alejandra Nuñez-Leal, M., Ramírez-Hernández, J., Mejía-Trejo, A., & Rosas-Verdugo, E. (2019). Seismic noise levels in northern Baja California, Mexico. *Bulletin of the Seismological Society of America*, *109*(2), 610–620. https://doi.org/10.1785/0120180155

Ramírez-Ramos, E. E., Vidal-Villegas, A., González-Fernández, A., & Stock, J. M. (2015). A Crustal Velocity Model for the Southern Mexicali Valley, Baja California, Mexico. *Seismological Research Letters*, *86*(1), 181–191. https://doi.org/10.1785/0220140007

Reyes, L. M., Rebollar, C. J., & Castro, R. (2001). Depth of the Moho in northern Baja California using (Pg-Pn) travel times. *Geofísica Internacional*, *40*(1), 1–9. https://doi.org/10.22201/igeof.00167169p.2001.40.1.417

Stock, J. M., Martín-Barajas, A., Suárez-Vidal, F., & Miller, M. M. (1991). Miocene to Holocene extensional tectonics and volcanic stratigraphy of NE Baja California, Mexico. In *Geological excursions in southern California and Mexico: Guide book* (pp. 21–24). 1991 Annual Meeting, Geological Society of America.

Suárez-Vidal, F., Mendoza-Borunda, R., Nafarrete-Zamarripa, L. M., Rámirez, J., & Glowacka, E. (2008). Shape and dimensions of the Cerro Prieto pull-apart basin, Mexicali, Baja California, Mexico, based on the regional seismic record and surface structures. *International Geology Review*, *50*(7), 636–649. https://doi.org/10.2747/0020-6814.50.7.636

Vidal-Villegas, J. A., Munguía, L., González-Ortega, J. A., Nuñez-Leal, M. A., Ramírez, E., et al. (2018). The Northwest Mexico Seismic Network: Real-Time Seismic Monitoring in Northern Baja California and Northwestern Sonora, Mexico. *Seismological Research Letters*, *89*(2A), 324–337. https://doi.org/10.1785/0220170183

Wetmore, P. H., Malservisi, R., Fletcher, J. M., Alsleben, H., Wilson, J., Callihan, S., et al. (2019). Slip history and the role of the Agua Blanca fault in the tectonics of the North American-Pacific plate boundary of southern California, USA and Baja California, Mexico. *Geosphere*, *15*(1), 119–145. https://doi.org/10.1130/GES01670.1

Zhu, L., & Kanamori, H. (2000). Moho depth variation in southern California from teleseismic receiver functions. *Journal of Geophysical Research: Solid Earth*, *105*(B2), 2969–2980. https://doi.org/10.1029/1999JB900322

Zhu, L., Mitchell, B. J., Akyol, N., Cemen, I., & Kekovali, K. (2006). Crustal thickness variations in the Aegean region and implications for the extension of continental crust. *Journal of Geophysical Research*, *111*(B1). https://doi.org/10.1029/2005JB003770